

Global Hopf Bifurcation in the ZIP regulatory system

Juliane Claus · Mariya Ptashnyk ·
Ansgar Bohmann · Andrés
Chavarría-Krauser

Received: date / Accepted: date

Abstract Regulation of zinc uptake in roots of *Arabidopsis thaliana* has recently been modeled by a system of ordinary differential equations based on the uptake of zinc, expression of a transporter protein and the interaction between an activator and inhibitor. For certain parameter choices the steady state of this model becomes unstable upon variation in the external zinc concentration. Numerical results show periodic orbits emerging between two critical values of the external zinc concentration. Here we show the existence of a global Hopf bifurcation with a continuous family of stable periodic orbits between two Hopf bifurcation points. The stability of the orbits in a neighborhood of the bifurcation points is analyzed by deriving the normal form, while the stability of the orbits in the global continuation is shown by calculation of the Floquet multipliers. From a biological point of view, stable periodic orbits lead to potentially toxic zinc peaks in plant cells. Buffering is believed to be an efficient way to deal with strong transient variations in zinc supply. We extend the model by a buffer reaction and analyze the stability of the steady state in dependence

Send offprint requests to: A. Chavarría-Krauser

This work was supported by the German Research Foundation, grant number CH 958/1-1 and by the Excellence Initiative II, Heidelberg University, “Mobilitätsmaßnahmen im Rahmen internationaler Forschungsk Kooperationen 2013-2014”, project number D.80100/13.009.

J. Claus
Interdisciplinary Center for Scientific Computing, Heidelberg University
E-mail: juliane.claus@bioquant.uni-heidelberg.de

M. Ptashnyk
Division of Mathematics, University of Dundee
E-mail: mptashnyk@maths.dundee.ac.uk

A. Bohmann
Interdisciplinary Center for Scientific Computing, Heidelberg University

A. Chavarría-Krauser
Interdisciplinary Center for Scientific Computing, Heidelberg University
E-mail: andres.chavarria@bioquant.uni-heidelberg.de

of the properties of this reaction. We find that a large enough equilibrium constant of the buffering reaction stabilizes the steady state and prevents the development of oscillations. Hence, our results suggest that buffering has a key role in the dynamics of zinc homeostasis in plant cells.

Keywords transport processes in plants · zinc uptake · Hopf bifurcation · periodic orbits · stability

1 Introduction

Zinc is an essential micronutrient for plants, because it plays an important role in many enzymes catalyzing vital cellular reactions. In higher doses, however, zinc is toxic. Therefore, plants have to strictly control and adjust the uptake of zinc through their roots depending on its concentration in the surrounding soil. This is achieved by a complicated control system consisting of sensors, transmitters and zinc transporter proteins.

The main influx transporters of zinc are proteins of the ZIP (zinc-, iron-responsive proteins) family (Grotz et al., 1998; Guerinot, 2000). They were shown to be highly expressed under conditions of zinc deficiency and down-regulated under zinc excess (Talke et al., 2006). The mechanism of this regulation has been studied by Assunção et al. (2010a). They showed that *ZIP4* in *Arabidopsis thaliana* is regulated by the transcription factors bZIP19 and bZIP23 of the basic-region leucine zipper (bZIP) family. These transcription factors apparently induce ZIP expression by binding to a zinc deficiency response element (ZDRE), which is present in the promoter region of most ZIP proteins. Thereby, bZIPs increase ZIP transporter expression under zinc deficiency. When the internal zinc concentration in the cell rises, bZIPs are inhibited and the expression of zinc transporters decreases strongly. The mechanistic details of this inhibition are yet unclear, as bZIP transcription factors do not seem to have a zinc binding site for sensing the internal zinc concentration (Assunção et al., 2010a). Most likely there are additional sensors that bind zinc and inhibit bZIP19 and bZIP23 (Assunção et al., 2010b).

These biological observations gave rise to a mathematical model, which we developed and published previously in Claus and Chavarría-Krauser (2012). The interested reader finds more details on the model, notation, parameters and biological implications there. The model is a four-dimensional autonomous system of ordinary differential equations

$$\begin{aligned} \frac{du}{dt} &= F(u, \mu), \quad t \in [0, \infty), \\ u(0) &= u^0, \end{aligned} \tag{1}$$

with a parameter $\mu \in \mathcal{M} := [0, m]$, where $m > 0$ sufficiently large, a C^1 function $F : \mathbb{R}^4 \times \mathcal{M} \rightarrow \mathbb{R}^4$, and non-negative initial conditions $u^0 \in \mathbb{R}_+^4$. Referring to the original notation of Claus and Chavarría-Krauser (2012), the components of u are the gene expression level, internal zinc concentration, the

activation and inhibition levels, and the parameter μ represents the external zinc concentration. In this paper we study the qualitative behavior of the solutions with respect to the parameter μ .

Dynamical systems depending on a parameter μ can undergo bifurcations that change the qualitative behavior of solutions substantially when crossing a critical value μ^* . In the Hopf (or Poincaré-Andronov-Hopf) bifurcation, first described by Hopf (1942), a steady state changes stability as a pair of complex conjugate eigenvalues of the linearization cross the imaginary axis and a family of periodic orbits bifurcates from the steady state.

While the original results by Hopf (1942) give conditions for the local existence of such orbits, later works are focused on the global continuation of periodic solutions. The first result on global continuability of periodic orbits for ordinary differential equations was presented in Alexander and Yorke (1978) using methods of algebraic topology. Another proof of the global result was given in Ize (1976) using homotopy theory. The Fuller index, an index for periodic solutions of a system of autonomous equations, was used in Chow and Mallet-Paret (1978) to generalize the global Hopf bifurcation theorem, proved by Alexander and Yorke (1978), to functional differential equations. An *orbit index* and a *center index* were introduced in Mallet-Paret and Yorke (1982) and applied also in Alligood et al. (1983) to analyze the large connected sets of periodic solutions of a one-parameter differential equation. Hopf bifurcation points with a center index of 1 are called *sources*, and those with center index of -1 are called *sinks*. Mallet-Paret and Yorke (1982) showed, that if a set of orbits is bounded with respect to the parameter, solution, and periods of the orbits, then the set must have as many source as sink Hopf bifurcations. Each source is connected to a sink by an oriented one-parameter path of orbits that contains no orbits with zero orbit index. The results on global continuability for locally continuable non-Möbius orbits of general C^1 dynamical systems were obtained in Alligood and Yorke (1984). The term “global” Hopf bifurcation is sometimes used to denote only unbounded sets of periodic solutions (Fiedler, 1986). We, however, will use it in the sense of Alexander and Yorke (1978) to mean any non-local continuation of a family of periodic orbits.

The paper is organized as follows. In Sect. 2 we consider the well-posedness and uniform boundedness of the solutions, and prove the existence of a unique stationary solution of the model for the regulation of zinc uptake. Then, we shall show in Sect. 3 that for two critical parameter values μ_1 and μ_2 Hopf bifurcations occur in the model. By deriving the normal form in Sect. 4, we analyze the stability of the periodic orbits in a neighborhood of the bifurcation points. Furthermore, in Sect. 5 we show the existence of a global continuous path of periodic orbits between the two Hopf bifurcation points and in Sect. 6 analyze the stability of periodic solutions by calculating the Floquet multipliers via the monodromy matrix. Finally, in Sect. 7, we extend the model by a buffer reaction and analyze the properties needed to ensure the stability of the stationary solutions.

2 Mathematical model

In Claus and Chavarría-Krauser (2012) we studied mathematical models for the regulation of ZIP transporters in response to external zinc concentration. The most promising model identified in this study included a dimerizing activator A , as well as an inhibitor I that senses the internal zinc concentration Z and inhibits the activator. Gene activity (denoted by G) is induced by the activator and leads to transcription of mRNA (M) and production of ZIP transporter proteins (T).

We consider a simplification of the original system, where transcription and translation of transporter proteins are assumed to be quasi-stationary and in equilibrium $G = M = T$. Thereby, the system reduces to four equations describing the time evolution of G , Z , A , and I , now denoted by u_1 , u_2 , u_3 , and u_4 , respectively. The non-dimensionalized model reads

$$\begin{aligned}\frac{du_1}{dt} &= \kappa u_3^2(1 - u_1) - u_1, \\ \frac{du_2}{dt} &= u_1 f(\mu) - u_2, \\ \frac{du_3}{dt} &= 1 - \gamma_1 u_3 u_4 - u_3, \\ \frac{du_4}{dt} &= \gamma_2 u_2 - \gamma_3 u_3 u_4 - (1 + \gamma_2 u_2) u_4,\end{aligned}\tag{2}$$

where $f(\mu) := \frac{\mu}{\mu + K}$ defines the influx of zinc dependent on the external zinc concentration μ . The parameter κ describes the induction of gene activity (u_1) by the dimerized activator (u_3), γ_1 and γ_3 the binding between activator and inhibitor (u_3 and u_4), γ_2 the binding between zinc (u_2) and the inhibitor (u_4), and K is the Michaelis constant of the reaction between external zinc (μ) and zinc transporters (u_1). All parameter values, here $K = 13$, $\kappa = 20$, $\gamma_1 = 380$, $\gamma_2 = 1000$, $\gamma_3 = 1672$, have been estimated from literature and by fitting the model to experimental data (Claus and Chavarría-Krauser, 2012). As a property of the soil, the external zinc concentration is considered as the bifurcation parameter $\mu \in \mathcal{M}$.

Considering $F(u, \mu) = (F_1(u), F_2(u, \mu), F_3(u), F_4(u))^T$, where

$$\begin{aligned}F_1(u) &= \kappa u_3^2(1 - u_1) - u_1, & F_2(u, \mu) &= u_1 f(\mu) - u_2, \\ F_3(u) &= 1 - \gamma_1 u_3 u_4 - u_3, & F_4(u) &= \gamma_2 u_2 - \gamma_3 u_3 u_4 - (1 + \gamma_2 u_2) u_4,\end{aligned}$$

we can rewrite the system (2) in the form (1). $F(u, \mu)$ is continuously differentiable in u and its Jacobian is given by

$$J(u, \mu) = \begin{pmatrix} -\kappa u_3^2 - 1 & 0 & 2\kappa u_3(1 - u_1) & 0 \\ f(\mu) & -1 & 0 & 0 \\ 0 & 0 & -\gamma_1 u_4 - 1 & -\gamma_1 u_3 \\ 0 & \gamma_2(1 - u_4) & -\gamma_3 u_4 & -\gamma_3 u_3 - 1 - \gamma_2 u_2 \end{pmatrix}.\tag{3}$$

Theorem 1 *For any initial value $u^0 \in \mathcal{S}$, where $\mathcal{S} = [0, 1]^4$, there exists a unique global solution $u \in C^\infty([0, \infty) \times \mathcal{M})$ of the system (2) and $u(t, \mu) \in \mathcal{S}$ for all $t \in [0, \infty)$ and any $\mu \in \mathcal{M}$.*

Proof Due to the local Lipschitz continuity of F , we obtain the local in time existence and uniqueness of a solution $u(t, \mu)$ of (2) by the Picard-Lindelöf theorem.

To prove the uniform boundedness of the solution, we show that \mathcal{S} is a positively invariant region for the system (2), i.e. that any trajectory $u(t, \mu)$ with $u(0, \mu) \in \mathcal{S}$ remains in \mathcal{S} for all times $t \geq 0$. From the equations of the system (2) and by using the positivity of the coefficients we obtain the following estimates

$$\begin{aligned} F_1(u)|_{u_1=0} &= \kappa u_3^2 \geq 0, & F_2(u)|_{u_2=0} &= u_1 f(\mu) \geq 0 & \text{for } u_1 \geq 0, \\ F_3(u)|_{u_3=0} &= 1 > 0, & F_4(u)|_{u_4=0} &= \gamma_2 u_2 \geq 0 & \text{for } u_2 \geq 0, \end{aligned}$$

which by applying the invariant region theorem (Theorem 14.7 in Smoller, 1994; Amann, 1990, Theorem 16.9) with $G_i(u) = -u_i$, for $i = 1, 2, 3, 4$, imply the lower bound $u \geq 0$. To show the upper bound we use the fact that $f(\mu) < 1$ and obtain

$$\begin{aligned} F_1(u)|_{u_1=1} &= -1 \leq 0, & F_2(u)|_{u_2=1} &= u_1 f(\mu) - 1 \leq 0 \text{ for } u_1 \leq 1, \\ F_3(u)|_{u_3=1} &= -\gamma_1 u_4 \leq 0 \text{ for } u_4 \geq 0, & F_4(u)|_{u_4=1} &= -\gamma_3 u_3 - 1 \leq 0 \text{ for } u_3 \geq 0. \end{aligned}$$

Then with $G_i(u) = u_i - 1$ the invariant region theorem ensures that $u_i \leq 1$, for $i = 1, 2, 3, 4$. Thus, any trajectory starting in \mathcal{S} remains bounded within this set. The global existence and uniqueness of a solution of (2) is then implied by the uniform boundedness of $u(t, \mu)$ together with continuous differentiability of F . The smoothness of $F : \mathbb{R}^4 \times \mathcal{M} \rightarrow \mathbb{R}^4$ with respect to u and μ ensures also the smoothness of the solutions u of the system (2) (Amann, 1990).

Theorem 2 *For any positive parameter set κ, K, γ_1 to γ_3 and μ , there exists a unique steady state $u^*(\mu)$ of the system (2) in $\mathcal{S} = [0, 1]^4$. Furthermore, $u^* \in C^\infty((0, \infty))$. In particular, the steady state is isolated.*

The proof of Theorem 2 will be based on the following two Lemmata. In these, $f := \frac{\mu}{\mu + K}$ will be used as parameter instead of μ and K , as for any $K \in (0, \infty)$ the function $f(\mu)$ is bijective in $[0, \infty)$ and every $f \in (0, 1)$ is uniquely identified with a $\mu \in (0, \infty)$. We assume $\kappa, \gamma_1, \gamma_2, \gamma_3 \in (0, \infty)$ and denote the parameter space by $\mathcal{P} := (0, 1) \times (0, \infty)^4$ with elements $p = (f, \kappa, \gamma_1, \gamma_2, \gamma_3) \in \mathcal{P}$.

Lemma 1 *For any $p \in \mathcal{P}$ the system (2) has at least one steady state $u^* \in \text{int } \mathcal{S}$ and none on $\partial \mathcal{S}$. Further, any steady state $u^* \in \text{int } \mathcal{S}$ corresponds to a root u_3^* in $\mathcal{S}_3 := \left(\frac{1}{1+\gamma_1}, 1\right)$ of the polynomial*

$$\begin{aligned} \phi(x) &:= \gamma_3 \kappa x^4 + (f \gamma_2 (1 + \gamma_1) + 1 - \gamma_3) \kappa x^3 \\ &\quad + (\gamma_3 - \kappa - f \gamma_2 \kappa) x^2 + (1 - \gamma_3) x - 1, \end{aligned} \tag{4}$$

and any root of ϕ in \mathcal{S}_3 to precisely one steady state in $\text{int } \mathcal{S}$.

Proof Existence of u^* follows from Brouwer's fixed point theorem (Smoller, 1994, cf. Theorem 12.10), since \mathcal{S} is a positively invariant (see Theorem 1), compact and convex subset of \mathbb{R}^4 .

A steady state u^* in \mathcal{S} is a solution of $F(u^*, p) = 0$. Equation $F_3(u^*, p) = 0$ implies $u_3^* > 0$. Using $F_1(u^*, p) = 0$ to $F_3(u^*, p) = 0$, expressions for u_1^* , u_2^* , and u_4^* as functions of u_3^* are found:

$$u_1^* = \frac{\kappa u_3^{*2}}{1 + \kappa u_3^{*2}}, \quad u_2^* = \frac{f \kappa u_3^{*2}}{1 + \kappa u_3^{*2}}, \quad u_4^* = \frac{1 - u_3^*}{\gamma_1 u_3^*}. \quad (5)$$

Note that u_1^* and u_2^* increase whereas u_4^* decreases strictly monotonously with u_3^* . In particular we have $u_2^* > 0$, as $f > 0$ and $u_3^* > 0$. Assuming $u_4^* = 0$ or $u_4^* = 1$ leads to a contradiction in $F_4(u^*, p) = 0$, and hence, to $u_4^* \in (0, 1)$. The last equation in (5) delivers a monotonic expression for u_3^* in dependence of u_4^* . From monotonicity it follows that u_3^* as a function of u_4^* assumes its extrema at the bounds of $(0, 1)$, and thus, $u_3^* \in \mathcal{S}_3$. Correspondingly, by monotonicity of u_1^* and u_2^* with respect to u_3^* , we find $u_1^*, u_2^* \in (0, 1)$. Thus, $u^* \in \text{int } \mathcal{S}$ and $u^* \notin \partial \mathcal{S}$ for any $p \in \mathcal{P}$.

Substituting (5) into $F_4(u^*, p) = 0$ yields the equation $\phi(u_3^*) = 0$. Thus, any steady state $u^* \in \text{int } \mathcal{S}$ corresponds to a root of ϕ in \mathcal{S}_3 . Conversely, if u_3^* is a root of ϕ in \mathcal{S}_3 , then (5) delivers unique u_1^* , u_2^* and u_4^* , which fulfill $F(u^*, p) = 0$ and $u^* \in \text{int } \mathcal{S}$.

Lemma 2 *The number of steady states of system (2) in \mathcal{S} is constant for all $p \in \mathcal{P}$, and the determinant of the Jacobian (3) is strictly positive when evaluated at a steady state $u^* \in \mathcal{S}$.*

Proof Consider $D := \det J(u^*, p)$ where u^* is a steady state corresponding to the parameter p . The relations (5) may be used to express u_1^* , u_2^* , and u_4^* by u_3^* , and the determinant is then

$$D = \frac{1}{x(1 + \kappa u_3^{*2})} \left(\gamma_3 \kappa^2 u_3^{*6} + (\kappa f \gamma_2 + 2\gamma_3 + \kappa) \kappa u_3^{*4} + (2\kappa + \gamma_3) u_3^{*2} + 1 \right. \\ \left. + (2f\gamma_2(1 + \gamma_1)u_3^* - f\gamma_2) \kappa u_3^{*2} \right),$$

where $u_3^* \in \mathcal{S}_3$ as defined as in Lemma 1. Up to $-f\gamma_2$, all terms are positive. Using $u_3^* > \frac{1}{1+\gamma_1}$ we find

$$2f\gamma_2(1 + \gamma_1)u_3^* - f\gamma_2 > f\gamma_2 > 0.$$

Thus, $D > 0$ for any $p \in \mathcal{P}$ and any corresponding steady state $u^* \in \mathcal{S}$.

Since \mathcal{P} is connected and \mathbb{N} is discrete, the number of steady states in \mathcal{S} could only be non-constant if it was discontinuous in \mathcal{P} . By Lemma 1 a steady state u^* cannot enter or leave the compact set \mathcal{S} upon variation of p , because any steady u^* depends continuously on p and does not cross over $\partial \mathcal{S}$. Hence, the only way the number of steady states could change is by bifurcation of steady states (pitchfork or saddle node), which is not possible because $D > 0$ in \mathcal{P} . In total, we find that the number of steady states in \mathcal{S} has to be constant for any $p \in \mathcal{P}$.

Proof (Theorem 2) By choosing one specific parameter in \mathcal{P} , namely $f = \frac{1}{2}$ and $\kappa = \gamma_1 = \gamma_2 = \gamma_3 = 1$, we obtain

$$\phi(x) = x^4 + x^3 - \frac{1}{2}x^2 - 1,$$

and $\mathcal{S}_3 = (\frac{1}{2}, 1)$. We find the existence of at least one root because $\phi(\frac{1}{2}) = -\frac{15}{16} < 0$ and $\phi(1) = \frac{1}{2} > 0$. The uniqueness is proven by strict monotonicity of ϕ in \mathcal{S}_3 :

$$\frac{d\phi}{dx} = 4x^3 + 3x^2 - x > \frac{1}{4} > 0.$$

By Lemma 1 this corresponds to exactly one steady state in \mathcal{S} and from Lemma 2 the same holds for any $p \in \mathcal{P}$.

The smoothness of u^* with respect to p follows from the smoothness of F and the implicit function theorem. As f is given by a smooth function in μ (for $\kappa, \gamma_1, \gamma_2, \gamma_3, K$ fixed), the steady state $u^*(\mu)$ can also be viewed as a smooth function in μ .

3 Local Hopf bifurcation

In numerical simulations of the model (2) with sufficiently high values of the parameter γ_1 we observe a stable steady state for small μ , which becomes unstable at some critical parameter value μ_1 and stable again after some value $\mu_2 > \mu_1$ (Claus and Chavarría-Krauser, 2012). Between these values, i.e. for $\mu \in (\mu_1, \mu_2)$, numerical simulations of the system (2) show the existence of stable limit cycles depending continuously on μ . In this section we show that at both critical values of μ a Hopf bifurcation occurs and study the stability of the emerging periodic orbits. Since experiments have shown that external zinc concentrations above 30 μM are lethal for *A. thaliana* (Talke et al., 2006), from now on we will use $m = 30$, i.e. $\mathcal{M} = [0, 30]$. The model parameters are chosen as in Sect. 2.

Theorem 3 *There exist two critical values $\mu_1, \mu_2 \in \mathcal{M}$ of the external zinc concentration for which a Hopf bifurcation occurs in the system (2).*

Proof We shall show that all criteria for existence of a local Hopf bifurcation (Hopf, 1942; Hassard et al., 1981) are satisfied by the system (2). The right hand side $F : \mathbb{R}^4 \times \mathcal{M} \rightarrow \mathbb{R}^4$ of (2) is continuously differentiable in u and μ . Theorem 2 guarantees the existence of a unique equilibrium $u^*(\mu)$ inside the invariant set \mathcal{S} . Using Newton and continuation methods we find numerically an explicit family of unique positive stationary solutions $u^*(\mu)$ of (2). By Theorem 2 the equilibrium $u^*(\mu)$ is isolated.

From the continuity of $f(\mu) = \frac{\mu}{\mu+K}$, of $u^*(\mu)$ with respect to μ , and of the determinant, we obtain that the eigenvalues $\lambda_i(\mu)$, $i = 1, 2, 3, 4$, of the Jacobian $J(u^*(\mu), \mu)$ evaluated at the stationary solution, vary continuously with μ .

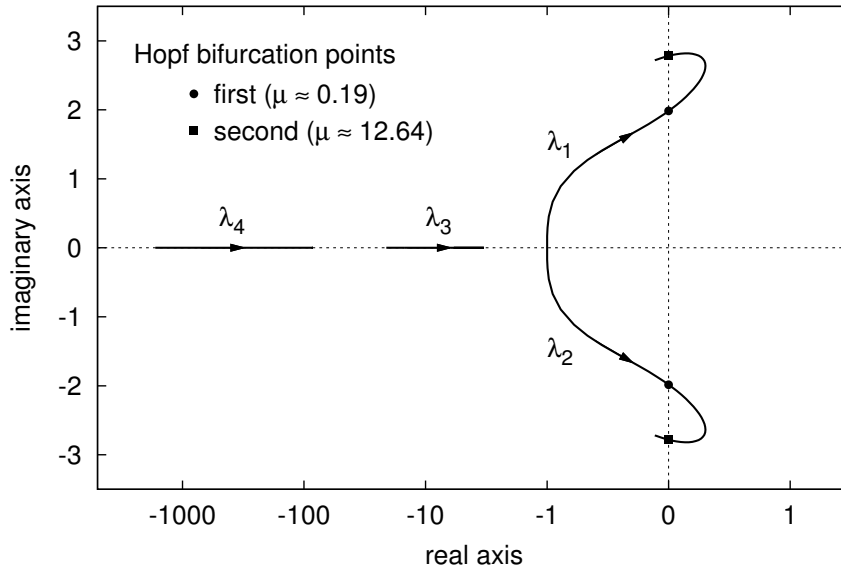


Fig. 1 Eigenvalues of the Jacobian matrix of F at the steady state for varying external zinc concentrations between 0 and 30. Arrows show the direction of increasing external zinc concentration. The eigenvalues λ_3 and λ_4 are real and negative for the entire range of external zinc concentrations, while the complex conjugate pair $\lambda_{1,2}$ crosses the imaginary axis twice. These points are marked as first and second Hopf bifurcation points.

A diagram of these eigenvalues in the complex plane for different values of μ is shown in Fig. 1. For $\mu = 0$ the eigenvalues can be calculated explicitly and are equal to $\lambda_{1,2} = -1$, $\lambda_3 = -\kappa - 1 = -21$ and $\lambda_4 = -\gamma_3 - 1 = -1673$. For $\mu \in (0, 30]$ the eigenvalues were computed numerically by a reduction of the Jacobian matrix to Hessenberg form followed by QR iteration as described in Press et al. (2007).

The two smallest eigenvalues λ_3 and λ_4 have negative real parts for all $\mu \in \mathcal{M} = [0, 30]$, while λ_1 and λ_2 form a complex conjugate pair that crosses the imaginary axis in two points (Fig. 1). The values of $\lambda_1, \dots, \lambda_4$ for the critical parameter points $\mu_1 = 0.189537\dots$ and $\mu_2 = 12.6432\dots$ at which $J(u^*(\mu), \mu)$ exhibits two purely imaginary eigenvalues are shown in Table 1. The purely imaginary eigenvalues $\lambda_{1,2}(\mu_i)$ are simple and none of the multiples $n \lambda_{1,2}(\mu_i)$, with $n \in \mathbb{N} \setminus \{1\}$, is an eigenvalue of $J(u^*(\mu_i), \mu_i)$ for $i = 1, 2$. This follows from $\det J(u^*(\mu_i), \mu_i) > 0$ and $\text{tr} J(u^*(\mu_i), \mu_i) < 0$ which imply $\lambda_{3,4}(\mu_i) < 0$. The eigenvalues $\lambda_{1,2}(\mu)$ cross the imaginary axis with non-zero speed, i.e. $\frac{d}{d\mu} \text{Re} \lambda_i(\mu_j) \neq 0$ for $i, j = 1, 2$, which was verified numerically (Table 1).

Therefore, based on the Hopf Bifurcation Theorem (Hopf, 1942; Hassard et al., 1981) we conclude that the system (2) has a one-parameter family of periodic solutions in a neighborhood of both critical values μ_1 and μ_2 , bifurcating from the stationary solution.

Table 1 Critical values of μ with the corresponding eigenvalues $\lambda_1, \dots, \lambda_4$ of the Jacobian matrix, derivative of the real part of the eigenvalue with respect to μ and sign of the real part of the parameter b in the normal form.

	value of μ	$\lambda_{1,2}$	λ_3	λ_4	$\frac{d}{d\mu} \operatorname{Re}(\lambda_{1,2})$	$\operatorname{sgn}(\operatorname{Re} b)$
μ_1	0.189...	$\pm i1.983\dots$	-3.474...	-238.6...	1.83...	-1
μ_2	12.64...	$\pm i2.782\dots$	-5.599...	-84.43...	-0.0126...	-1

4 Derivation of the normal form and stability of Hopf bifurcation

In the last section we showed the existence of periodic orbits in the neighborhood of the two Hopf bifurcation points. Further information is needed to determine the stability and direction of the periodic solutions.

Theorem 4 *At both critical parameter values μ_1 and μ_2 a supercritical Hopf bifurcation occurs for the system (2) and the bifurcating periodic solutions are stable. In the first critical point μ_1 the orbits arise for increasing values $\mu > \mu_1$, whereas in the second critical point μ_2 the orbits arise for decreasing values $\mu < \mu_2$.*

Proof In order to apply the results known from literature, we shift the critical parameter value and stationary solution to zero by setting $\tilde{\mu} = \mu - \mu^*$, $\tilde{u} = u - u^*(\tilde{\mu} + \mu^*)$ and rewrite (2) as

$$\frac{d\tilde{u}}{dt} = F(\tilde{u} + u^*(\tilde{\mu} + \mu^*), \tilde{\mu} + \mu^*) . \quad (6)$$

As F is smooth, by Haragus and Iooss (2011, Theorems 2.9, 3.3) and Ipsen et al. (1998) and using the results of Theorem 3, we conclude that the system (6) possesses a two-dimensional center manifold for sufficiently small $\tilde{\mu}$. Eq. (6) reduced on this manifold is transformed by a specific polynomial transformation into the normal form (Hassard et al., 1981)

$$\frac{dA}{dt} = i\omega A + a\tilde{\mu}A + bA|A|^2 + \mathcal{O}\left(|A|(|\tilde{\mu}| + |A|^2)^2\right) . \quad (7)$$

The solutions of (6) on the center manifold are then of the form

$$\tilde{u} = A\xi + \overline{A}\bar{\xi} + \Psi(A, \bar{A}, \tilde{\mu}), \quad A(t) \in \mathbb{C} , \quad (8)$$

with $\Psi(0, 0, 0) = 0$, $\partial_A \Psi(0, 0, 0) = 0$, and $\partial_{\bar{A}} \Psi(0, 0, 0) = 0$, where ξ is the eigenvector of $J(u^*, \mu^*)$ for the purely imaginary eigenvalue $\lambda_1 = i\omega$. For $\Psi(A, \bar{A}, \tilde{\mu})$ a polynomial ansatz

$$\Psi(A, \bar{A}, \tilde{\mu}) = \sum \psi_{rsq} A^r \bar{A}^s \tilde{\mu}^q, \quad (9)$$

with $\psi_{100} = \psi_{010} = 0$ and $\psi_{rsq} = \bar{\psi}_{srq}$ is made (Haragus and Iooss, 2011). Substituting the form (8) for u into equations (6) we obtain

$$\begin{aligned} (\xi + \partial_A \Psi) \frac{dA}{dt} + (\bar{\xi} + \partial_{\bar{A}} \Psi) \frac{d\bar{A}}{dt} \\ = F(A\xi + \bar{A}\bar{\xi} + \Psi(A, \bar{A}, \tilde{\mu}) + u^*(\tilde{\mu} + \mu^*), \tilde{\mu} + \mu^*) . \end{aligned} \quad (10)$$

Knowing the first term in the Taylor expansion of F at $\tilde{\mu} = 0$ and $\tilde{u} = 0$ to be $F(u^*(\mu^*), \mu^*) = 0$ we get

$$\begin{aligned} F(\tilde{u} + u^*(\tilde{\mu} + \mu^*), \tilde{\mu} + \mu^*) &= D^{10}F \cdot \tilde{u} + D^{10}F \cdot \partial_\mu u^* \tilde{\mu} + D^{01}F \tilde{\mu} \\ &+ \frac{1}{2} D^{20}F(\tilde{u}, \tilde{u}) + D^{11}F \cdot \tilde{u} \tilde{\mu} + \frac{1}{2} D^{20}F(\partial_\mu u^*, \partial_\mu u^*) \tilde{\mu}^2 \\ &+ \frac{1}{2} D^{10}F \cdot \partial_\mu^2 u^* \tilde{\mu}^2 + \frac{1}{2} D^{02}F \tilde{\mu}^2 + \dots , \end{aligned} \quad (11)$$

where $\tilde{u} = A\xi + \bar{A}\bar{\xi} + \Psi(A, \bar{A}, \tilde{\mu})$ and the derivatives are defined by

$$D^{pq}F := \left. \frac{\partial^{p+q} F(u, \mu)}{\partial u^p \partial \mu^q} \right|_{(u^*(\mu^*), \mu^*)} .$$

As before, we write $J = D^{10}F(u^*(\mu^*), \mu^*)$. Higher order derivatives in u are multilinear forms $D^{20}F : (\mathbb{C}^n)^2 \rightarrow \mathbb{C}^n$ and $D^{30}F : (\mathbb{C}^n)^3 \rightarrow \mathbb{C}^n$, with $n = 4$. These forms are applied to $x, y, z \in \mathbb{C}^n$ to obtain vectors in \mathbb{C}^n where the i -th components are given by

$$\begin{aligned} (D^{20}F(x, y))_i &:= \sum_{j,k}^n \frac{\partial^2 F_i}{\partial u_j \partial u_k} x_j y_k , \\ (D^{30}F(x, y, z))_i &:= \sum_{j,k,l}^n \frac{\partial^3 F_i}{\partial u_j \partial u_k \partial u_l} x_j y_k z_l . \end{aligned}$$

For F in the system (2) the second and third derivatives $D^{20}F(x, y)$ and $D^{30}F(x, y, z)$, where $x, y, z \in \mathbb{C}^4$, are given by

$$D^{20}F(x, y) = \begin{pmatrix} -2\kappa u_3^*(x_1 y_3 + x_3 y_1) + 2\kappa(1 - u_1^*)x_3 y_3 \\ 0 \\ -\gamma_1(x_3 y_4 + x_4 y_3) \\ -\gamma_2(x_2 y_4 + x_4 y_2) - \gamma_3(x_3 y_4 + x_4 y_3) \end{pmatrix}$$

and

$$D^{30}F(x, y, z) = \begin{pmatrix} -2\kappa(x_1 y_3 z_3 + x_3 y_1 z_3 + x_3 y_3 z_1) \\ 0 \\ 0 \\ 0 \end{pmatrix} .$$

Using now the Taylor expansion (11) of F together with the expression (9) for Ψ and (7) in the equation (10), and comparing the coefficients in front of powers of A , \bar{A} and $\tilde{\mu}$ we obtain

$$\begin{aligned}\mathcal{O}(A) : \quad (i\omega - J)\xi &= 0, \\ (i\omega - J)\bar{\xi} &= 0.\end{aligned}$$

This is the eigenvalue problem for the Jacobian of F in $(u^*(\mu^*), \mu^*)$ for purely imaginary eigenvalues $i\omega, -i\omega$. Further on, we find:

$$\mathcal{O}(\tilde{\mu}) : \quad -J\psi_{001} = D^{01}F + D^{10}F \cdot \partial_{\mu}u^*, \quad (12)$$

$$\mathcal{O}(\tilde{\mu}A) : \quad (i\omega - J)\psi_{101} = -a\xi + D^{20}F(\xi, \psi_{001}) + D^{11}F \cdot \xi. \quad (13)$$

The solvability condition for the equation (13) is that its right hand side should be orthogonal to the kernel of the adjoint operator $-i\omega - J^*$. Thus we conclude

$$a \langle \xi, \xi^* \rangle = \langle D^{20}F(\xi, \psi_{001}) + D^{11}F\xi, \xi^* \rangle, \quad (14)$$

where $\langle \cdot, \cdot \rangle$ denotes the Hermitian scalar product, $J^* = J^T$ is the adjoint matrix (or simply transposed, since J is real) to J and ξ^* is the adjoint eigenvector to $-i\omega$ fulfilling $J^*\xi^* = -i\omega\xi^*$, scaled with a complex factor to ensure $\langle \xi, \xi^* \rangle = 1$. For more details see Haragus and Iooss (2011). Considering the fact that J is invertible and solving the equation (12) for ψ_{001} we can calculate the parameter a in the normal form using formula (14).

Considering now higher order terms in A and \bar{A} we obtain

$$\mathcal{O}(A^2) : \quad (2i\omega - J)\psi_{200} = \frac{1}{2}D^{20}F(\xi, \xi), \quad (15)$$

$$\mathcal{O}(|A|^2) : \quad -J\psi_{110} = D^{20}F(\xi, \bar{\xi}), \quad (16)$$

$$\begin{aligned}\mathcal{O}(A|A|^2) : \quad b\xi + (i\omega - J)\psi_{210} &= D^{20}F(\xi, \psi_{110}) + D^{20}F(\bar{\xi}, \psi_{200}) \\ &+ \frac{1}{2}D^{30}F(\xi, \xi, \bar{\xi}).\end{aligned} \quad (17)$$

The solvability condition for equation (17) yields

$$b \langle \xi, \xi^* \rangle = \left\langle D^{20}F(\xi, \psi_{110}) + D^{20}F(\bar{\xi}, \psi_{200}) + \frac{1}{2}D^{30}F(\xi, \xi, \bar{\xi}), \xi^* \right\rangle. \quad (18)$$

Since $2i\omega$ and 0 are not eigenvalues of J , we can solve equations (15) and (16) for ψ_{200} and ψ_{110} , respectively, and determine the constant b by formula (18).

Due to the normal form theory for dynamical systems, the sign of the real part of b determines the type of the Hopf bifurcation and stability of the emerging periodic solutions. If $\text{Re } b < 0$, stable periodic orbits arise at the side of the bifurcation where the steady state becomes unstable. This is called a *supercritical* Hopf bifurcation. A *subcritical* Hopf bifurcation occurs if the real part of b is positive and unstable orbits arise at the side of the bifurcation where the steady state is stable.

Applying standard numerical methods like Newton's and continuation methods used to compute stationary solutions and eigenvalues of the Jacobian matrix in Sect. 3, as well as LU decomposition (Press et al., 2007) for the matrices in (15), (16) and (18), we obtain b for the critical parameter values μ_1 and μ_2 . For both critical values of the parameter, $\operatorname{Re} b$ is negative (Table 1). Consequently, both Hopf bifurcations are supercritical and the families of periodic orbits are stable. The sign of the derivative $\frac{d}{d\mu} \operatorname{Re} \lambda_1(\mu_i)$, $i = 1, 2$ determines the direction in which the orbits appear. In the first critical point they arise to the right ($\mu_1 < \mu$), while at the second they emerge to the left ($\mu < \mu_2$), as clearly seen in Fig. 2.

5 Global continuation of a family of periodic solutions

While the results in Sect. 3 only give the existence of stable periodic orbits in a small neighborhood of the critical values of μ , we shall now show the existence of a continuous path of periodic orbits between those two bifurcation points. We shall use here the results on the global continuation of periodic orbits obtained by Alexander and Yorke (1978) and Mallet-Paret and Yorke (1982). It was shown for a system of ordinary differential equations with continuously differentiable nonlinear function F that a family of periodic orbits bifurcating from the stationary solution at a Hopf point can be continuously extended and become unbounded with respect to parameter μ , period T , or solution u , or converge to another Hopf point (Theorem A in Alexander and Yorke (1978), Theorem 4.1, Propositions 5.1, 5.2 and Snake Termination Principle in Mallet-Paret and Yorke (1982)).

We shall say that $(u^*(\mu^*), \mu^*)$ is a Hopf point if the condition of the Hopf Bifurcation Theorem are satisfied.

Theorem 5 *The model (2) possesses a continuous path of periodic solutions connecting two Hopf bifurcation points, where the first Hopf point $(u^*(\mu_1), \mu_1)$ is a source and the second Hopf point $(u^*(\mu_2), \mu_2)$ is a sink for the path.*

Proof We shall show in the following that for the model (2) neither parameter nor period nor solution can become unbounded, so the path of periodic orbits bifurcating from the stationary solution must end in an another Hopf point. Lemma 1 ensures uniform boundedness of solutions of the model (2). The parameter $\mu \in \mathcal{M}$ is naturally bounded, since zinc concentrations in the soil only appear within a certain range. The least period T of the orbits is a continuous function of μ . Numerical computations show that the period is also bounded for all $\mu \in [\mu_1, \mu_2]$, see Fig. 3 (a).

Thus, since parameter, period and solution remain bounded, and the domain \mathcal{M} of the parameter contains exactly two bifurcation points, the path of periodic orbits emerging from one Hopf point must terminate in another Hopf point, see Mallet-Paret and Yorke (1982, Propositions 5.1, 5.2). Therefore, there exists a continuous family of periodic solutions between those two

Hopf points. An illustration of this path of periodic orbits in two dimensions is given in Fig. 2.

Following the notation in Mallet-Paret and Yorke (1982), the center index $\#$ can be calculated to distinguish so-called “sources” from “sinks” of the path and to give a direction to the path of orbits connecting two Hopf points. The center index is defined as

$$\#(u^*(\mu^*), \mu^*) = \chi(-1)^{E(\mu^*)},$$

where $E(\mu)$ denotes the sum of the multiplicities of the eigenvalues of the Jacobian matrix $J(u^*(\mu), \mu)$ having strictly positive real parts. The number χ is the crossing number denoting the net number of pairs of eigenvalues crossing the imaginary axis at μ^* , defined by

$$\chi = \frac{1}{2}(E(\mu^*+) - E(\mu^*-)),$$

where $E(\mu^*+)$ and $E(\mu^*-)$ denote right- and left-hand limits of E at μ^* . In our case, exactly two eigenvalues cross the imaginary axis in the critical values $\mu_{1,2}$ and at μ_1 the two eigenvalues cross the imaginary axis from left to right, whereas at μ_2 they cross the imaginary axis from right to left. So we obtain $\chi = 1$ for μ_1 and $\chi = -1$ for μ_2 . Then with $E(\mu_{1,2}) = 0$ we find $\#(u^*(\mu_1), \mu_1) = +1$, so the first Hopf point (left point in Fig. 2) is a “source” of the path of periodic orbits. For the second Hopf point (right point in Fig. 2) we obtain $\#(u^*(\mu_2), \mu_2) = -1$, showing that it is a “sink”. This result is in concord with the Snake Termination Principle by Mallet-Paret and Yorke (1980) stating that if a path of orbits emerging from one Hopf point terminates in a second Hopf point, then the two Hopf points must have center indexes of opposite sign.

6 Floquet multipliers and stability of periodic orbits

The stability of periodic solutions can be analyzed by studying its Floquet multipliers. These multipliers can be derived as eigenvalues of the linearized Poincaré map and equivalently as eigenvalues of the monodromy matrix. In the following, we will focus on the latter.

Theorem 6 *The periodic solutions of the model (2) for $\mu \in [\mu_1, \mu_2]$ are asymptotically stable.*

Proof In the previous section we have shown that for a given $\mu \in [\mu_1, \mu_2]$ the system of differential equations (2) has a periodic solution $u(t) = u(\mu, t)$ with a period $T = T(\mu) \in (0, \infty)$. Naturally, all integer multiples of T are also periods, so T is chosen to be the least period. The periodic orbit is called asymptotically stable, if trajectories starting near the orbit converge to the orbit for $t \rightarrow \infty$. This stability is determined by the eigenvalues of the monodromy matrix of the system (2). For $\mu \in [\mu_1, \mu_2]$ the function $\Phi_t(u^0, \mu)$ denotes the solution $u(t)$

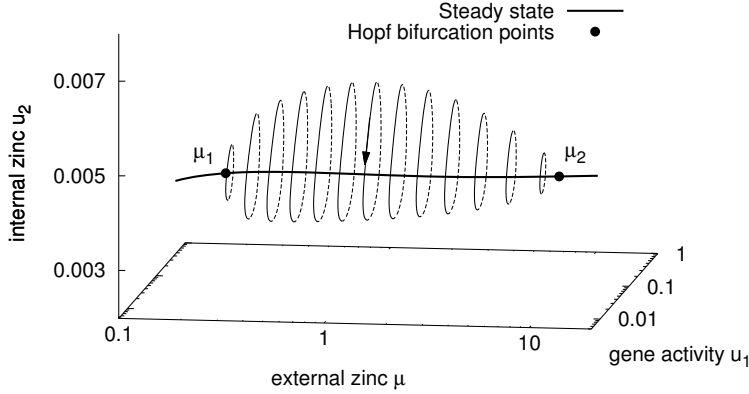


Fig. 2 Illustration of the path of periodic orbits between the two Hopf bifurcation points $(u^*(\mu_1), \mu_1)$ and $(u^*(\mu_2), \mu_2)$. From the four-dimensional system only two dimensions (gene activity and internal zinc concentration) are shown. The thick solid line marks the steady state, thin lines show the stable periodic solutions. The rotation direction is indicated with an arrow.

at time t starting from $u(0) = u^0$. For a point $(u^0(\mu), \mu)$ on a periodic orbit of (2) and the least period of this orbit $T = T(\mu)$, the monodromy matrix is given by

$$M = \frac{\partial \Phi_T(u, \mu)}{\partial u} \Big|_{u=u^0(\mu)}.$$

The eigenvalues of the monodromy matrix are called Floquet multipliers or characteristic multipliers. The Floquet multipliers are independent of the choice of u^0 on the periodic orbit, whereas the monodromy matrix and its eigenvectors depend on this choice. Since for $\mu \in [\mu_1, \mu_2]$ the system (2) possesses a periodic solution, one of the multipliers is always 1 and its eigenvector points in the direction tangential to the periodic cycle, i.e. $F(u^0)$ (Marx and Vogt, 2011). The periodic solution is asymptotically stable, if absolute values of all other Floquet multipliers are strictly smaller than 1 (Lust, 2001).

In order to numerically compute the Floquet multipliers we first obtain $u^0(\mu)$ and $T(\mu)$ using the single shooting technique (Marx and Vogt, 2011). For $\mu \in [\mu_1, \mu_2]$ and all points $u^0(\mu) \in \mathbb{R}^4$ on a periodic orbit with period $T(\mu)$ it holds that

$$g(u^0(\mu), T(\mu)) := \Phi_T(u^0(\mu), \mu) - u^0 = 0.$$

Since every point on a given orbit fulfills this equation, the system is underdetermined and an additional scalar “phase condition” of the form

$$h(u^0(\mu), T(\mu)) = 0$$

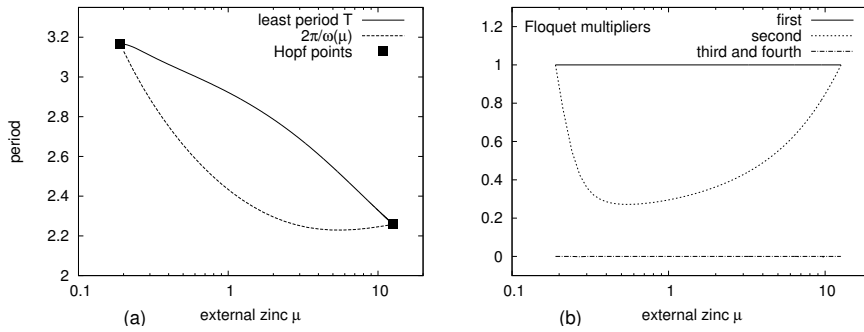


Fig. 3 Least period $T(\mu)$ (a) and Floquet multipliers (b) of periodic orbits as a function of the external zinc concentration μ between the two Hopf bifurcation points. (a) The numerically computed least period T (solid line) is shown together with the hypothetical period $2\pi/\omega$ of the linearized system in the steady state (dashed line), where ω is the imaginary part of the first eigenvalue of the Jacobian matrix J . At the critical bifurcation parameter values ($\mu_1 \approx 0.19$ and $\mu_2 \approx 12.6$) the lines cross, showing $\lim_{\mu \rightarrow \mu^*} T = 2\pi/\omega$. (b) Floquet multipliers were computed numerically. While the first Floquet multiplier equals one, the others are smaller than one. Therefore, the periodic solutions are of type 0 and asymptotically stable for all external zinc concentrations within this range.

is needed. Most simply, the condition fixes one of the components of the vector $u^0(\mu)$. Here, we estimated the stable periodic orbit by long-time numerical integration of the dynamical system (2) by starting slightly off the steady state $u^*(\mu)$. Then the state $u(\tau, \mu)$ for some large enough $\tau \in (0, \infty)$ was used to fix the component $u_1^0(\mu)$ by setting $h(u^0(\mu), T(\mu)) := u_1^0(\mu) - u_1(\tau, \mu)$. The combined system

$$g(u^0(\mu), T(\mu)) = 0, \quad h(u^0(\mu), T(\mu)) = 0$$

was solved for $(u^0(\mu), T(\mu)) \in \mathbb{R}^5$ with a standard Newton algorithm using $u(\tau, \mu)$ and a rough estimate $T(\mu)$ as starting values. Numerical integration of (2) was done with a Rosenbrock stiffly stable ODE solver (Press et al., 2007). For regular periodic solutions, the Newton iteration converges locally with quadratic rate (Marx and Vogt, 2011, Theorem 6.25). Having $u^0(\mu)$ and $T(\mu)$, the derivatives in the monodromy matrix were obtained by the finite difference formula and eigenvalues of the monodromy matrix were calculated using Hessenberg form and QR iteration as in Sect. 3.

The resulting minimal periods are shown in Fig. 3(a), while the Floquet multipliers for varying external zinc concentration $\mu \in [\mu_1, \mu_2]$ are shown in Fig. 3(b). As confirmed by the theory, the first multiplier in the direction tangent to the periodic orbit equals unity, while the others are real positive and smaller than one. Therefore, the periodic orbits are asymptotically stable for all external zinc concentrations between the two Hopf bifurcation points $(u^*(\mu_1), \mu_1)$ and $(u^*(\mu_2), \mu_2)$. In the bifurcation points, the second Floquet multiplier tends to unity and a conclusion on stability cannot be drawn. However, stability there is guaranteed by the normal form (see Sect. 3). Since

all of the multipliers besides the first are smaller than one in modulus for $\mu \in (\mu_1, \mu_2)$, no secondary bifurcation takes place and all the periodic orbits are of type 0 (Mallet-Paret and Yorke, 1982). It is also noteworthy that two of the Floquet multipliers are very close to zero. This shows that the periodic solutions are strongly attracting in two directions and corresponds to the two large negative eigenvalues of the Jacobian matrix J of the system (2).

7 Effects of buffering

In a recent paper (Claus and Chavarría-Krauser, 2013) we showed that stability of the steady state is affected by buffering. It changes the dynamical features of the system and its stability without changing the actual steady state values. Here, we want to discuss this in more detail.

Buffering is modeled with a simple extension to the system (2) based on a buffering reaction as described in Claus and Chavarría-Krauser (2013). The buffer is assumed to be present in high excess with almost constant concentration. In terms of the differential equations, a new equation

$$\frac{du_5}{dt} = p_2(p_1 u_2 - u_5), \quad (19)$$

is needed to account for the buffered zinc concentration denoted here as u_5 . The equilibrium constant p_1 gives the steady state ratio of buffered to unbuffered zinc concentrations, i.e. $p_1 = \frac{u_5^*}{u_2^*}$. The constant p_2 is the characteristic time of the buffering reactions in relation to the other reactions.

The equation for the internal zinc concentration u_2 needs to be extended to balance the buffering of zinc

$$\frac{du_2}{dt} = u_1 f(\mu) - u_2 - p_2(p_1 u_2 - u_5), \quad (20)$$

while the other equations in (2) remain unchanged. The first four components of the stationary solution, i.e. u_1^* , u_2^* , u_3^* , u_4^* , are unaffected by the extension and remain the same as for system (2). The steady state buffered zinc concentration is simply proportional to the internal zinc concentration ($u_5^* = p_1 u_2^*$). The dynamic behavior of the system, however, changes dramatically. We want to analyze this change with respect to the two buffering parameters $p = (p_1, p_2)$.

Most informative for the dynamical behavior of the system around the steady state is the largest eigenvalue of the Jacobian matrix. The Jacobian matrix of the extended system with buffering evaluated at the steady state is given by

$$J_b(u^*(\mu), \mu) = - \begin{pmatrix} a & 0 & -b & 0 & 0 \\ -c & 1 + p_1 p_2 & 0 & 0 & -p_2 \\ 0 & 0 & d & e & 0 \\ 0 & -f & g & h & 0 \\ 0 & -p_1 p_2 & 0 & 0 & p_2 \end{pmatrix} \quad (21)$$

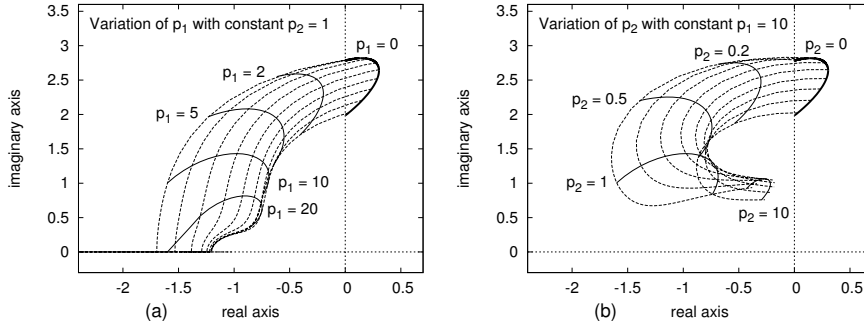


Fig. 4 First eigenvalue λ_1 of the Jacobian matrix J_b of the buffered system for variations of the two buffering parameters (a) p_1 and (b) p_2 . Dashed lines show isolines for constant external zinc concentration μ in the originally unstable region between 0.18 and 12.6. Constant lines mark isolines for constant p_1 (a) or p_2 (b), respectively. Increasing either p_1 (a) or p_2 (b) stabilizes the system by decreasing real and imaginary part of the eigenvalue.

where positive numbers a, b, c, d, e, f, g, h are introduced for simplification:

$$\begin{aligned} a &= \kappa(u_3^*)^2 + 1, & b &= 2\kappa u_3^*(1 - u_1^*), \\ c &= f(\mu), & d &= \gamma_1 u_4^* + 1, \\ e &= \gamma_1 u_3^*, & f &= \gamma_2(1 - u_4^*), \\ g &= \gamma_3 u_4^*, & h &= \gamma_3 u_3^* + 1 + \gamma_2 u_2^*. \end{aligned}$$

These values appeared already in the Jacobian matrix J of the unbuffered system [compare (3)]. The characteristic polynomial $\chi(\lambda, p)$ of J_b is

$$\chi(\lambda, p) = -bcf(\lambda + p_2) - (a + \lambda)(-eg + (d + \lambda)(h + \lambda)) \times (\lambda^2 + p_2 + \lambda(1 + p_2 + p_1 p_2)). \quad (22)$$

For an eigenvalue $\lambda(\mu, p)$ of J_b it holds that $\chi(\lambda(\mu, p), p) \equiv 0$ and $\frac{d\chi}{dp_i} \equiv 0$, $i = 1, 2$. Having the solution λ_i^0 of $\chi(\lambda(\mu, p), p) \equiv 0$ for $p_i = 0$ (no buffering), $i = 1, 2$, a continuation method can be applied

$$\begin{aligned} \frac{\partial \lambda}{\partial p_i} &= -\frac{\partial \chi}{\partial p_i} / \frac{\partial \chi}{\partial \lambda}, & p_i &\in [0, P_i], \\ \lambda(\mu, 0) &= \lambda_i^0, \end{aligned} \quad (23)$$

with $P_i > 0$, $i = 1, 2$ and $\mu \in \mathcal{M}$. This equation was solved numerically using a Dormand-Prince method with adaptive step size for solving ordinary differential equations (Press et al., 2007).

The effect of one of the buffering parameters can be calculated by choosing the other buffering parameter to be constant and by solving $\chi(\lambda(\mu, p), p) \equiv 0$ via (23) for a given μ . Fig.4 presents the simulation result for both parameters and for various external zinc concentrations $\mu \in \mathcal{M}$. Both an increase in p_1 and an increase in p_2 decreases the real part of the two complex eigenvalues below zero and leads to stability of the steady state for all external zinc

concentrations. In biological terms this means that buffering needs to be sufficiently strong (high p_1) and sufficiently fast (high p_2) to stabilize the system. Equilibrium constants $p_1 > 1.1$ ensure asymptotic stability of the stationary solution. Indeed, experimental measurements suggest that most zinc in the cells is bound to chelators and buffers (Dittmer et al., 2009; Vinkenborg et al., 2009), so p_1 can be estimated to be in the range of at least 1000. Under such high values of p_1 all eigenvalues are real and negative, and oscillations do not occur (Fig. 4a). The constant p_2 does not seem to play such an important role. The eigenvalues turn negative already at $p_2 \approx 0.09$ and increasing p_2 beyond 1 results even in less damping (Fig. 4b).

Until now, we analyzed how buffering changes the stability of the system for different values of μ . However, we have not dealt with the dynamic reaction to variations of μ . This parameter is the external zinc concentration, which tends to vary in time under natural soil conditions. To get an idea of how dynamic variation of μ affects the system, assume that the buffer reaction is such that the system stays near the steady state. Further, assume that variation in μ is small around a given μ^0 . Under these conditions, the linearized system reflects the behavior of the full system sufficiently well and the concept of the transfer function of linear time invariant systems can be applied. We denote with $u^0 := u^*(\mu^0)$ the steady state u^* for $\mu = \mu^0$. The input is $x := (\mu - \mu^0)/\mu^0$, while $y := (u_2 - u_2^0)/u_2^0$ is the output. In other words, the variation in external zinc concentration is the input and the output is given by the variation in internal zinc concentration. Note that the input and output were scaled to account for the difference in magnitude of u_2 and μ (~ 0.01 against ~ 1). The linearized system is then given by

$$\begin{aligned} \frac{d\tilde{u}}{dt} &= J_b^0 \tilde{u} + B^0 x, \\ y &= C^0 \cdot \tilde{u}, \end{aligned} \quad (24)$$

where $\tilde{u} = u - u^0$, $J_b^0 = J_b(u^0, \mu^0)$, $B^0 = \mu^0 \frac{\partial F}{\partial \mu}(u^0, \mu^0) = \mu^0 u_1^0 \partial_\mu f(\mu^0) \eta$, $\eta = (0, 1, 0, 0, 0)^T$ and $C^0 = \eta/u_2^0$.

Laplace transforming (24) renders

$$\mathcal{L}y = C^0 \cdot \left((sI - J_b^0)^{-1} B^0 \right) \mathcal{L}x,$$

where $\mathcal{L}y$ and $\mathcal{L}x$ are the Laplace transforms of y and x , respectively, and $s \in \mathbb{C}$. The function $G(s) := C^0 \cdot \left((sI - J_b^0)^{-1} B^0 \right)$ is the transfer function of the system. We determined $G(s)$ numerically for $\mu^0 = 1$, $p_2 = 1$ and various values of p_1 and present it in a Bode plot in Fig. 5. The details of how Fig. 5 was obtained follow. Firstly, the steady state of (2) extended by the equations (19) and (20) for the given μ^0 was determined. Secondly, J_b^0 , B^0 and C^0 were calculated for $p_2 = 1$ and various p_1 . Finally, $G(s)$ was calculated using GNU Octave's *Computer-Aided Control System Design* toolbox.

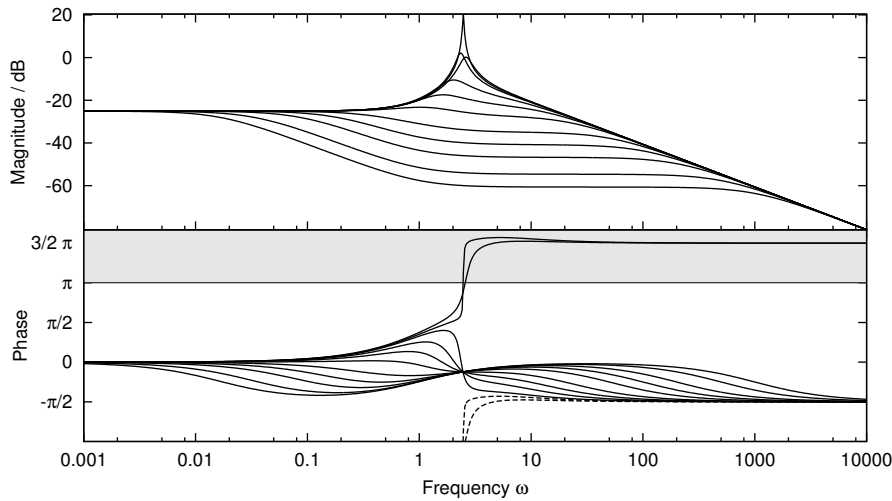


Fig. 5 Bode plot of the transfer function $G(s)$ of the system with buffering for $\mu^* = 1$, $p_2 = 1$ and various p_1 between 0 and 1000. For small p_1 below ~ 1.1 (unstable steady state) a clear resonance appears. The accumulated phases of the unstable cases go beyond π (grey box) and the corresponding principal values $\text{Arg } G(s)$ are shown as dashed lines.

Up to a resonance, the overall gain of the system is below -20 dB, and hence it is small (Fig. 5). Considering that the system is responsible for homeostasis of zinc, it makes sense that the gain is small to decouple the internal concentration as much as possible from the external concentration. A resonance at the frequency of the periodic orbits is clearly present for small p_1 , as expected from the results on the global Hopf bifurcation in Sect. 5. The accumulated phases in the phase response of these unstable cases go beyond π and tend to $\frac{3}{2}\pi$ for $\omega \rightarrow \infty$. Hence, the corresponding principal values $\text{Arg } G(s)$ are shown as dashed lines. Increasing p_1 damps the system until no Hopf bifurcations occur. This is seen by the sudden change in the phase response, where the argument of $G(s)$ stays smaller than π for all ω (Fig. 5 bottom). We found previously that high values of p_1 imply overdamping of the system (Fig. 4a). This fact is also reflected in the phase response for large p_1 : the phase for low frequencies becomes smaller than for moderate frequencies above the resonance frequency of the unbuffered system.

8 Conclusion and biological implications

Previous simulations showed that the zinc uptake and regulation model considered here tends to have periodic solutions for certain external zinc concentrations and parameter choices (Claus and Chavarría-Krauser, 2012). The true nature of the oscillation and the effect of buffering were not treated in that publication. Thus, we focused here on proving the existence and stability of

the periodic solutions and analyzed the effect of buffering by extending the model.

To reduce the complexity of the system we eliminated the purely linear equations from the original six-dimensional model and focused this analysis on four non-linear equations. For further reduction of the system's dimensionality one can look at the eigenvector belonging to the smallest eigenvalue λ_4 , i.e. the direction of fastest decay, see Sect. 3. Indeed, as part of the results it was found that this eigenvector points mainly in the direction of the inhibitor u_4 (data not shown). Thus, it is possible to further reduce the system to three dimensions by setting $\frac{du_4}{dt} = 0$ as a quasi steady state. Since the substitution of u_4 leads to more complicated equations and since the reduction of dimensions was not our main priority, we studied here the behavior of the four-dimensional system.

The naturally variable external zinc concentration μ was considered as the bifurcation parameter. The periodic orbits were found to bifurcate from stationary solutions $u^*(\mu)$ at two Hopf bifurcation points $(u^*(\mu_1), \mu_1)$ and $(u^*(\mu_2), \mu_2)$, where $\mu_1 \approx 0.19$ and $\mu_2 \approx 12.64$, and to form a continuous family of stable periodic solutions. By computing the Floquet multipliers the periodic solutions were found to be stable. Further, the transfer function of the linearized system was determined to analyze how the system reacts to dynamic variation in μ and how buffering influences this reaction. In an ideal homeostatic system the gain should be very low for all conditions to decouple the input and output. Here, we find indeed – up to a resonance corresponding to the frequency of the periodic solutions for low buffering – a low gain in general with very low values for high frequencies supporting the homeostatic property of the system.

From a biological point of view, it is assumed to be optimal for plants to keep an almost constant zinc concentration under wide ranges of external zinc supply. In the model, a high value of γ_1 , the binding affinity between activator and inhibitor, is required to make the steady state robust to variations in μ . Without buffering this high affinity, however, leads to a change in the system's dynamic behavior resulting in instability of the steady state and oscillations. Such oscillations generate toxic zinc peaks in the cells and therefore pose a dangerous threat for the plant. Without considering the important effect of buffering, we proposed that γ_1 should be smaller, yielding a model with less robust but stable steady states. Later results in Claus and Chavarría-Krauser (2013) and in this paper showed that stability can also be affected by buffering without changing the steady state. We found that already weak buffering can switch the dynamic behavior of the system from oscillations to a stable steady state and thus protect the plant cells against toxic zinc shocks. Thus, our results suggest that buffering is not only important as a mechanism against fast transient supply changes, but also to stabilize the regulatory system and prevent strong self-oscillatory behavior.

References

- J.C. Alexander and J.A. Yorke. Global bifurcations of periodic orbits. *Amer J Math*, 100(2):263–292, 1978.
- K.T. Alligood and J.A. Yorke. Families of periodic orbits: Virtual periods and global continuability. *J Differ Equations*, 55:59–71, 1984.
- K.T. Alligood, J. Mallet-Paret, and J.A. Yorke. An index for the global continuation of relatively isolated sets of periodic orbits. *Lect Notes Math*, 1007: 1–21, 1983.
- H. Amann. *Ordinary differential equations. An introduction to nonlinear analysis*. W. de Gruyter Berlin, 1990.
- A.G.L. Assunção, E. Herrero, Y.-F. Lin, B. Huettel, S. Talukdar, C. Smaczniak, R.G.H. Immink, M. van Eldik, M. Fiers, H. Schat, and M.G.M. Aarts. *Arabidopsis thaliana* transcription factors bZIP19 and bZIP23 regulate the adaptation to zinc deficiency. *PNAS*, 107(22):10296–10301, 2010a.
- A.G.L. Assunção, H. Schat, and M.G.M. Aarts. Regulation of the adaptation to zinc deficiency in plants. *Plant Signal Behav*, 5(12):1553–1555, 2010b.
- S.-H. Chow and J. Mallet-Paret. The Fuller index and global Hopf bifurcation. *J Differ Equations*, 29:66–85, 1978.
- J. Claus and A. Chavarría-Krauser. Modeling regulation of zinc uptake via ZIP transporters in yeast and plant roots. *PLoS One*, 7:e37193, 2012.
- J. Claus and A. Chavarría-Krauser. Implications of a zinc uptake and transport model. *Plant Signal Behav*, 8:e24167, 2013.
- P. J. Dittmer, J. G. Miranda, J. A. Gorski, and A. E. Palmer. Genetically encoded sensors to elucidate spatial distribution of cellular zinc. *J Biol Chem*, 284(24):16289–97, 2009.
- B. Fiedler. Global Hopf bifurcation of two-parameter flows. *Arch Ration Mech An*, 94(1):59–81, 1986.
- N. Grotz, T. Fox, E. Connolly, W. Park, M.L. Guerinot, and D. Eide. Identification of a family of zinc transporter genes from *Arabidopsis* that respond to zinc deficiency. *PNAS*, 95:7220–7224, 1998.
- M.L. Guerinot. The ZIP family of metal transporters. *Biochim Biophys Acta*, 1465:190–198, 2000.
- M. Haragus and G. Iooss. *Local Bifurcations, Center Manifolds, and Normal Forms in Infinite-Dimensional Dynamical Systems*. Springer London, 2011.
- B.D. Hassard, N.D. Kazarinoff, and Y.-H. Wan. *Theory and applications of Hopf bifurcation*. Cambridge Univ Pr, 1981.
- E. Hopf. Abzweigung einer periodischen Lösung von einer stationären Lösung eines Differentialsystems. *Ber Math Phys Kl Sachs Akad Wiss Leipzig*, 94: 1–22, 1942.
- M. Ipsen, F. Hynne, and P. G. Sørensen. Systematic derivation of amplitude equations and normal forms for dynamical systems. *Chaos*, 8:834–852, 1998.
- J. Ize. Bifurcation theory for Fredholm operators. *Mem Am Math Soc*, 7(174), 1976.
- K. Lust. Improved numerical Floquet multipliers. *Int J Bifurcat Chaos*, 11 (9):2389–2410, 2001.

- J. Mallet-Paret and J.A. Yorke. Two types of Hopf bifurcation points: sources and sinks of families of periodic orbits. *Ann N Y Acad Sci*, 357:300–304, 1980.
- J. Mallet-Paret and J.A. Yorke. Snakes: Oriented families of periodic orbits, their sources, sinks, and continuation. *J Differ Equations*, 43:419–450, 1982.
- B. Marx and W. Vogt. *Dynamische Systeme: Theorie und Numerik*. Spektrum Akademischer Verlag Heidelberg, 2011.
- W.H. Press, S.A. Teukolsky, W.T. Vetterling, and B.P. Flannery. *Numerical Recipes: The art of scientific computing*. Cambridge Univ Pr, third edition, 2007.
- J. Smoller. *Shock Waves and Reaction-Diffusion Equations*. Springer-Verlag New York, 1994.
- I.N. Talke, M. Hanikenne, and U. Krämer. Zinc-dependent global transcriptional control, transcriptional deregulation, and higher gene copy number for genes in metal homeostasis of the hyperaccumulator *Arabidopsis halleri*. *Plant Physiol*, 142:148–167, 2006.
- J. L. Vinkenborg, T. J. Nicolson, E. A. Bellomo, M. S. Koay, G. A. Rutter, and M. Merks. Genetically encoded FRET sensors to monitor intracellular Zn²⁺ homeostasis. *Nat Methods*, 6(10):737–40, 2009.